

CFD simulations of diesel multi-hole injector internal flow and spray jet development at increasing chamber pressure and temperature conditions

Charalambos Chasos*¹

¹Frederick University, 1036 Nicosia, Cyprus

*Corresponding author: eng.cca@frederick.ac.cy

Abstract

Strict emissions regulations and engine performance improvement requirements impose the development and use of high-pressure multi-hole diesel injectors, which are employed in direct-injection common rail systems of diesel internal combustion engines. The fuel injection and air/fuel mixing can be improved by increasing the injection pressure higher than two thousand bar. However, high injection pressures may cause cavitation and affect the initial spray characteristics, including jet shape and spray angle. The main objective of the present work was to investigate the effect of chamber pressure and temperature on the internal nozzle flow, on the initial liquid jet breakup length and on the jet angle at the vicinity of the nozzle exit. A typical diesel six-hole injector with nozzle holes symmetrically located around the periphery of the injector tip was designed and modelled. The nozzle diameter and length were 0.2 mm and 1 mm, respectively, with a ratio of nozzle orifice length over nozzle diameter L/D equal to 5. The symmetrical one-sixth segment of the injector at the nozzle tip was assembled with a constant volume chamber with square cross-sectional area with side 1 mm and a chamber length of 5 mm. A computational unstructured mesh of around one million prism cells was generated with the STAR-CD computational fluid dynamics (CFD) code. The transient CFD simulations were performed with the STAR-CD code, utilising the Eulerian methodology and the volume of fluid (VOF) method for the two-phase flow of liquid and gas, and using the Rayleigh cavitation model. CFD simulations were performed for an injection pressure of 2245 bar of liquid n-heptane which was injected in the constant volume chamber at increasing chamber pressure and temperature. Four test cases were investigated, including atmospheric chamber pressure and temperature, atmospheric pressure and chamber temperature of 700 K, and high chamber pressure of 42 bar at 700 and 1000 K chamber temperature, respectively. For all cases, cavitation occurs at the region of upper wall of the nozzle and affects the fuel/air mixing downstream the nozzle exit. The increase of chamber temperature slightly reduces the spray cone angle and has negligible effect on jet breakup length. The spray angle increases around 50 % when the chamber pressures increases by around 40 bar, and the spray angle decreases around 10% when the chamber temperature increases by 300 K. Comparisons of jet breakup length and the spray jet angle against empirical data showed moderately good agreement.

Keywords

Multi-hole diesel injector, CFD simulation, VOF method, cavitation, breakup length, spray jet angle, empirical data.

Introduction

The phenomenon of high-pressure diesel injection from diesel injector nozzles is very complex and the disintegration of the emerging jet requires further understanding. Modern high-pressure diesel injectors are of multi-hole type and have nozzles with a length over diameter ratio, L/D , ranging from approximately 4 to 6. The injection pressures applied in common rail injection systems can be higher than 2000 bar, and diesel fuel injection in engine cylinders takes place in high pressure and temperature conditions, during compression stroke in cylinders with high turbulence. The high injection pressure in combination with the sudden decrease of cross-sectional area at the vicinity of the diesel nozzle entry generates cavitation. The aim of the present work was to examine the effects of chamber pressure and temperature on the internal nozzle flow where cavitation occurs, the effects on the initial liquid jet breakup length and on the spray jet angle at the vicinity of the nozzle exit. Furthermore, it was the objective of the present was to characterize the effects chamber temperature and pressure on the pattern of the air/fuel mixture downstream the nozzle in the chamber.

The internal and external flows of diesel injectors were investigated in experimental [1, 10, 14, 15] and computational [1, 6, 9, 11, 13] studies, among others. The main findings from experiments carried out in transparent large scale injectors showed that cavitation occurs in the nozzle [10, 14], and that the spray jet at the vicinity of the nozzle exit is dictated by the cavitation upstream in the nozzle and the interaction with the ambient gas flow. Modelling and simulation studies examined the injector flow utilising the VOF methodology [8] and the

large eddy simulation methodology [5]. From simulations [8], it was found that strong vortex structures are generated around the liquid jet penetrating in the gas phase due to the velocity relaxation within the liquid jet inside and outside the nozzle. Also, the effects of injection pressure on the initial spray atomization characteristics were examined, and it was revealed that when the injection pressure increases, then both the breakup length and the downstream penetration of the spray jet increase, while the spray jet angle at the vicinity of nozzle exit slightly increases with increasing injection pressure.

For better understanding of diesel injection into varying chamber conditions, the present work used CFD simulations at constant high injection pressure and examined the effect of chamber temperature and pressure on the liquid jet breakup length, on the spray jet cone angle, and on the air/fuel mixture pattern within the constant volume chamber.

Methodology

The Eulerian modelling methodology included the mass, momentum and energy conservation equations for the two phases, employing the VOF method as it is implemented in the CFD code STAR-CD [3]. The interface-capturing method in the VOF method was used, which computes the convective terms in the volume fraction equations using the High-Resolution Interface-Capturing (HRIC) model [3]. For the two-phase flow modelling, the pressure in the two phases is assumed the same. Constant surface tension coefficient is used, with which the normal force due to the surface tension is treated using the continuum surface force (CSF) model [3], while the tangential force is not accounted. The CSF model provides a source term in the momentum conservation equation. The turbulence was modelled with the $k-\epsilon$ high Reynolds number RNG model [17], and the boundary layer was handled with the standard wall functions. The MARS [3] differencing scheme was used for the discretization of the conservation equations. The SIMPLE algorithm [3] was employed for the transient numerical solution of the problem.

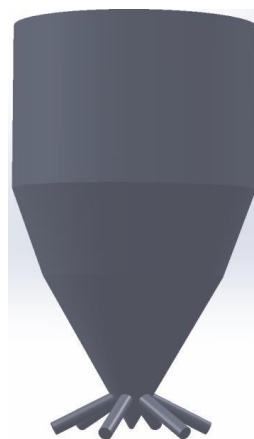


Figure 1. Three-dimensional injector geometry.

A VCO sac-less six-hole diesel injector was designed using published geometry details from typical multi-hole diesel injectors from literature ([10, 11, 14, 15]). The three-dimensional injector was designed with a CAD software [4] and it is illustrated in Figure 1. The nozzle entry has a sharp edge at the body of the injector. The injector nozzle diameter and length were 0.2 mm and 1 mm, respectively, with a ratio of nozzle orifice length over nozzle diameter $L/D = 5$.

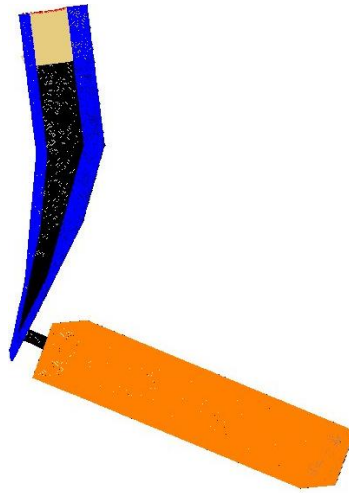


Figure 2. Computational mesh and boundary conditions.

A constant volume chamber was assembled at the nozzle exit tip, with a length of 5 mm and a square cross-sectional area with side width 1 mm. The constant volume chamber was assembled at the centreline of the nozzle and the symmetry axes of the chamber and the nozzle coincided. The computational mesh was generated with the automatic mesh generation tool of STAR-CD [3]. The resulting mesh was composed of around 850000 prism cells, and it is shown in Figure 2. The cell size was around 5 to 10 μm within the injector and between 10 to 20 μm in the chamber. Inlet boundary condition was defined at the entry of the injector on the top, presented in dark yellow color in Figure 2. Symmetry plane boundary conditions were imposed on the symmetry sides of the one-sixth segment of the injector, indicated with violet color in Figure 2. Slip wall boundary condition was imposed on the four sides of the chamber, presented with orange color in Figure 2. No-slip wall boundary condition was used at the injector body, at the injector needle and the back plane of the chamber wall where the nozzle was assembled. At the inlet boundary, the volume fraction of the fuel was set equal to 1, and uniform inlet velocity was defined. The injection pressure at the inlet of the injector was calculated by code using the inlet velocity. The fuel used was n-heptane, and the physical properties of liquid fuel, vapour fuel and air were taken from the database of STAR-CD [3] and are included in Table 1.

Table 1. Liquid/vapour fuel and air properties.

Property	Liquid n-heptane	Vapour n-heptane	Air
Density (Kg/m^3)	678.3	2.48639	1.18415
Molecular viscosity (Kg/ms)	$3.92073 \cdot 10^{-4}$	$1.01377 \cdot 10^{-5}$	$1.855 \cdot 10^{-5}$
Surface tension coefficient (N/m)	0.0727		

Pressure boundary condition was defined at the chamber front plane, where the different conditions of chamber pressure and temperature were defined for each test case.

For the transient simulations, stagnant air initial conditions were set in the computational domain. The simulations for the four test cases were performed for an injection duration of 1 ms with a constant time step size of 0.5 μs .

For the validation of the present simulations, empirical equations were used and empirical data was estimated for comparisons. The empirical equations provide the primary spray atomization characteristics, and can be used for the atomization modelling for diesel engines in the absence of experimental data. The empirical equations for the calculation of the breakup length and the spray angle were selected from [15] and [2], respectively.

The liquid jet breakup length was calculated with the equation from [2],

$$L = 0.39 (2 \Delta p / \rho_l)^{1/2} t \quad (1)$$

where Δp is the pressure drop along the nozzle, ρ_l is the liquid density and t is the elapsed time after the start of injection.

The diesel jet spray angle in the atomisation region was calculated by the equation from [2],

$$\theta = 0.017 \left(\frac{D^2 \rho_a \Delta p}{\mu_a^2} \right)^{0.25} \quad (2)$$

where D is the nozzle diameter, ρ_a is the density of air in the chamber and μ_a is the molecular viscosity of air.

Results

The simulation results obtained for the four test cases are presented and discussed in the current section. The injection pressure for the four test cases was constant and equal to 2245 bar, while the chamber pressure and temperature varied from atmospheric conditions to high pressure and temperature. The chamber pressure and temperature for the four test cases are included in Table 2. The injection pressure was calculated by the code at the inlet boundary using a constant liquid velocity of 28 m/s providing a fuel mass flow rate equal to 0.0592 Kg/s.

Table 2. Test cases operating conditions.

Test case	Description of chamber conditions	P_{ch} (bar)	T_{ch} (K)
1	Atmospheric	1	298
2	Atmospheric pressure and high temperature	1	700
3	High pressure and high temperature	42	700
4	High pressure and maximum temperature	42	1000

For the four test cases, firstly the simulation results are plotted and compared at the vertical symmetry section plane of computational domain. Then, comparisons of the breakup length and spray angle data estimated from the simulations against empirical data are presented.

Firstly, for the atmospheric chamber pressure, and increasing temperature from 298 to 700 K, the simulations comparison of the evolution of the VOF and velocity fields for the Cases 1 and 2 are presented in Figure 3 and 4. Then, the results of Cases 2 and 3 for constant chamber temperature of 700 K and increasing chamber pressure from 1 to 42 bar are presented Figure 5 and 6. Finally, the more realistic results resembling diesel engine cylinder conditions, for the Cases 3 and 4 at constant pressure of 42 bar and increasing temperature from 700 to 1000 K are compared in Figure 7 and 8. The plots of simulation results are indicated with the instance of time in ms after the start of injection (ASOI).

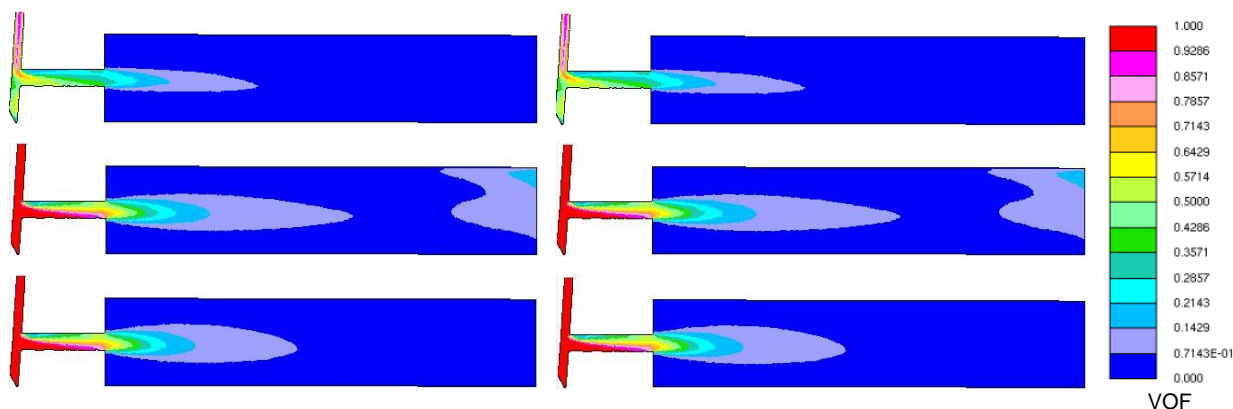


Figure 3. Comparison of the VOF field for the Cases 1 and 2, for chamber pressure 1 bar and temperature 298 K (left) and 700 K (right), at 0.15, 0.2 and 0.25 ms ASOI.

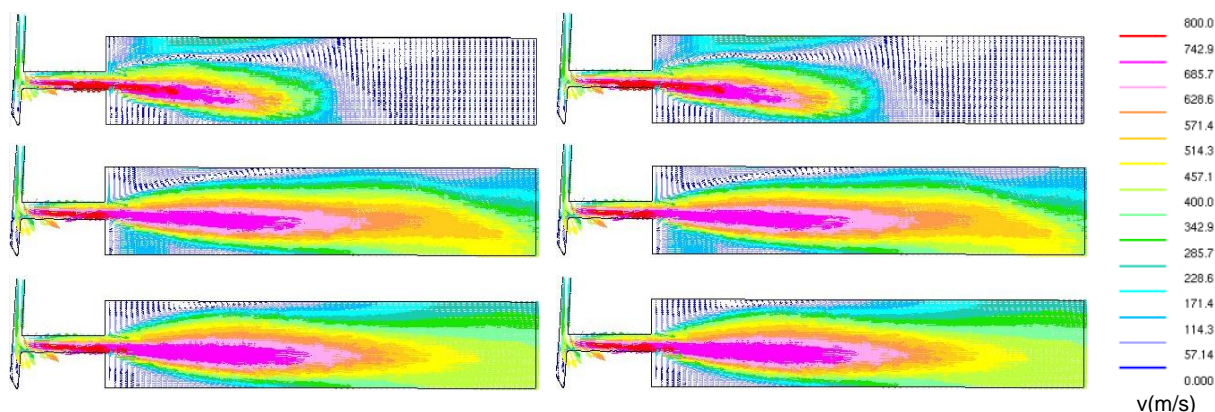


Figure 4. Comparison of the velocity field for the Cases 1 and 2, for chamber pressure 1 bar and temperatures 298 K (left) and 700 K (right), at 0.15, 0.2 and 0.25 ms ASOI.

The transient development of the spray jet can be observed in Figure 3 and 4 at 0.15, 0.2 and 0.25 ms ASOI. It can be seen that cavitation starts from the upper edge of the nozzle entry. Also, the cavitation pattern does not change after around 0.2 ms ASOI. The core of the spray jet has a quasi-steady pattern at the vicinity of the nozzle and it is slightly deflected towards downward, because of the interaction with the gas flow field in the chamber as it can be seen in Figure 4. Figure 3 shows that a slightly narrower jet is produced when the chamber temperature is increasing, because of the evaporation phenomenon which becomes stronger. However, the differences for increasing chamber temperature are negligible, as it is shown in both Figure 3 and 4.

The comparisons of the results examining the effect of the increasing chamber pressure on the VOF and the velocity fields for high temperature of 700 K, are included in Figure 5 and 6. When the chamber temperature increased, then the emerging jet downward deflection intensified at 0.15 ms ASOI as it is shown in Figure 5, and afterwards the jet radial spreading increased. It can be also observed that the jet which emerges in the chamber with higher pressure on the right in Figure 5 is more unstable and attenuates compared to jet of the low pressure. Also at lower pressure the jet is more symmetrical than the jet at higher pressure. The velocity field comparison is included in Figure 6 and shows that the gas velocity field becomes wider when the chamber pressure is decreased especially at areas where fuel is not present. This widening of the velocity field indicates that the spray jet penetrates faster at low chamber pressure than the spray jet at high chamber pressure. As it can be seen in Figure 5, at high pressure the fuel jet angle towards downstream is bigger than the jet angle at the low pressure, because of the instability and attenuation of the emerging the jet. The important observation is that the jet breakup length increases when the chamber pressure is increasing from approximately 1 mm to 1.5 mm, as it can be noticed at 0.25 ms ASOI.

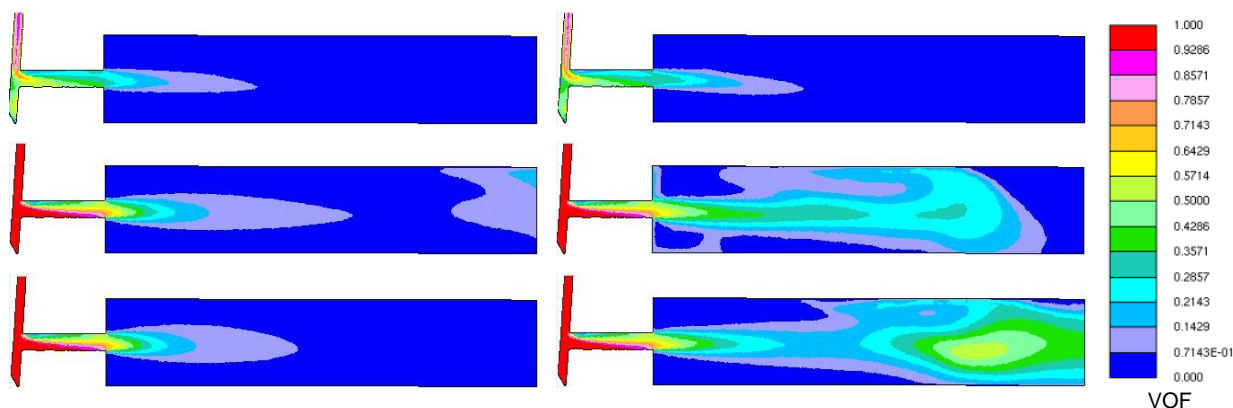


Figure 5. Comparison of the VOF field for the Cases 2 and 3, for constant chamber temperature of 700 K and increasing pressure from 1 bar (left) to 42 bar (right), at 0.15, 0.2 and 0.25 ms ASOI.

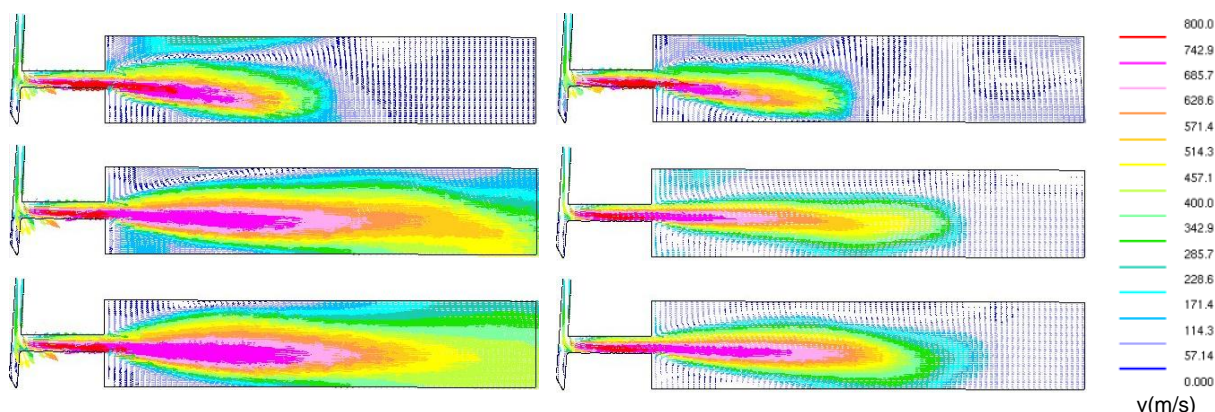


Figure 6. Comparison of the velocity field for the Cases 2 and 3, for constant chamber temperature of 700 K and increasing pressure from 1 bar (left) to 42 bar (right), at 0.15, 0.2 and 0.25 ms ASOI.

For the high pressure chamber condition of 42 bar and for increasing temperature from 700 to 1000 K, the plots of the VOF and velocity fields are compared in Figure 7 and 8. The results in Figure 7 and 8 are similar to the

results presented in Figure 3 and 4, where the jet at the highest temperature is slightly thinner, as well as the temperature increase has negligible effect on the resulting spray jet shape, breakup length and angle.

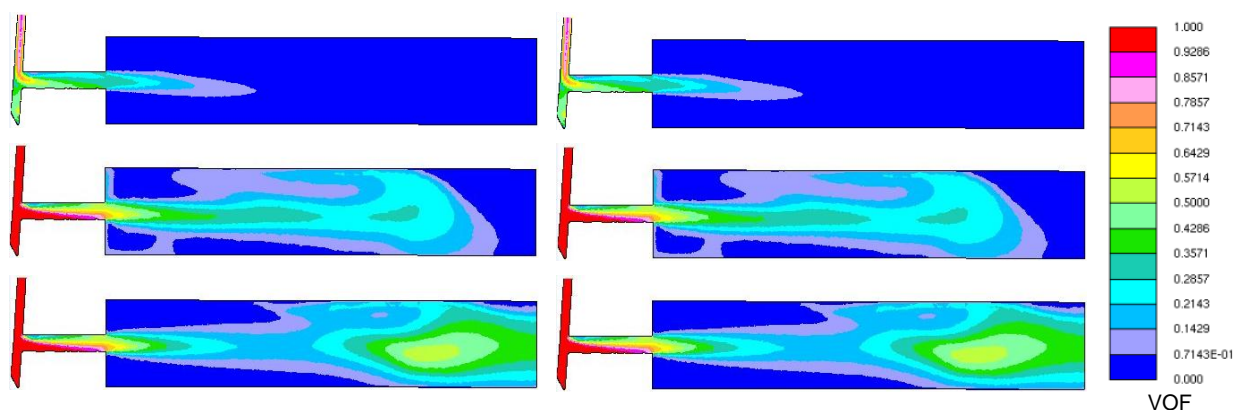


Figure 7. Comparison of the VOF field for the Cases 3 and 4, for chamber pressure 42 bar and temperatures 700 K (left) and 1000 K (right), at 0.15, 0.2 and 0.25 ms ASOI.

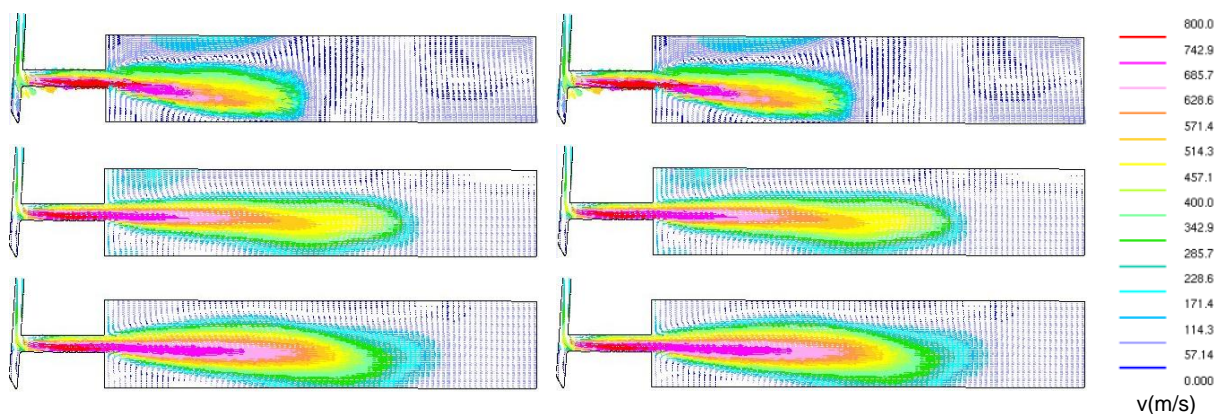


Figure 8. Comparison of the velocity field for the Cases 3 and 4, for chamber pressure 42 bar and temperatures 700 K (left) and 1000 K (right), at 0.15, 0.2 and 0.25 ms ASOI.

The main finding from the simulation results and their comparisons, was that the effect of chamber pressure is more intense on the resulting spray than the effect of chamber temperature. This phenomenon can be explained by the resulting chamber densities which affect the momentum transfer between the gas and the fuel liquid and vapour phases, along with the pertinent interactions within the chamber. It was generally observed that the cavitation pattern within the nozzle is not affected for the chamber temperature and pressure conditions which were examined in the present work.

The comparison of the breakup length estimated from the simulations for the cases at high chamber pressure against the breakup length empirical data is illustrated in Figure 9. The time of the start of injection was adjusted with the value of 0.14 ms, in order to account for the elapsed time from the start of simulation, which is required by that the jet to start emerging from the nozzle exit. From the simulation results, the breakup length was estimated at the distance from nozzle where the VOF value was equal and greater than 0.15, as it can be seen in the plots of Figure 7, at 0.15 ms and 0.2 ms, respectively. Figure 9 reveals that the breakup length data estimated from the simulation agrees very well with the empirical data at the early stages of injection at 0.01 ms ASOI. Both in the simulation and the empirical data, the breakup length increases with elapsed time, as it is shown in Figure 9. However, during the later period of spray injection, the liquid jet penetration is underpredicted. The underprediction is due to the evaporation phenomenon which is present and it is modelled by the simulation, while the empirical data does not account the evaporation phenomenon.

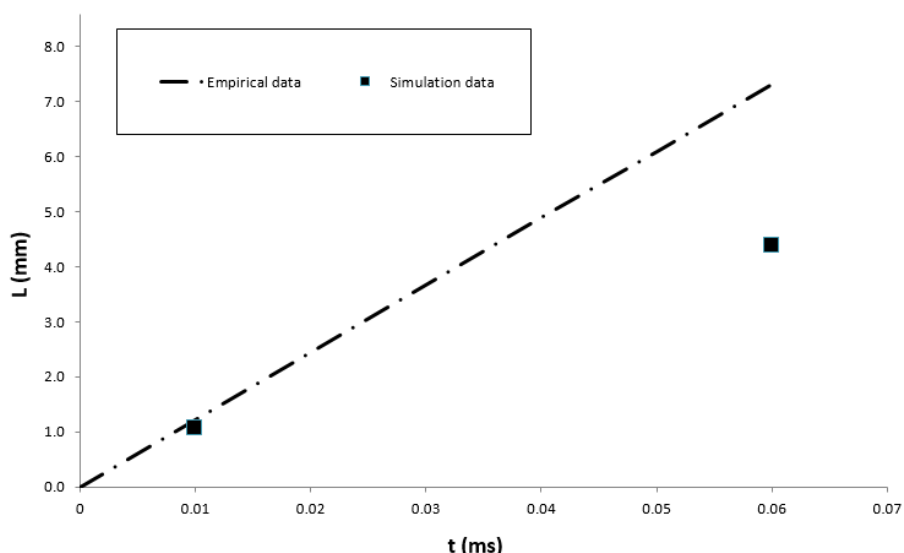


Figure 9. Comparison of the breakup length between the simulation and the empirical data with elapsed time ASOI, for chamber at high pressure.

From the simulations, the spray jet average angle was estimated at 0.25 ms ASOI, by using tangents from the nozzle exit upper and lower edges directed to the outer upper and lower edges of the jet spray at the distance of five nozzle diameters from the nozzle exit. The average spray jet angle for the cases of increasing chamber pressure from 1 to 42 bar at 700 K are compared with the empirical data in Figure 10. As it can be observed from Figure 10, the same trend of the spray angle increase with increasing chamber pressure is captured, both in the simulation and in the empirical data. Figure 10 also shows that the spray angle is underestimated at low chamber pressure, while at high chamber pressure is very well predicted by the simulation.

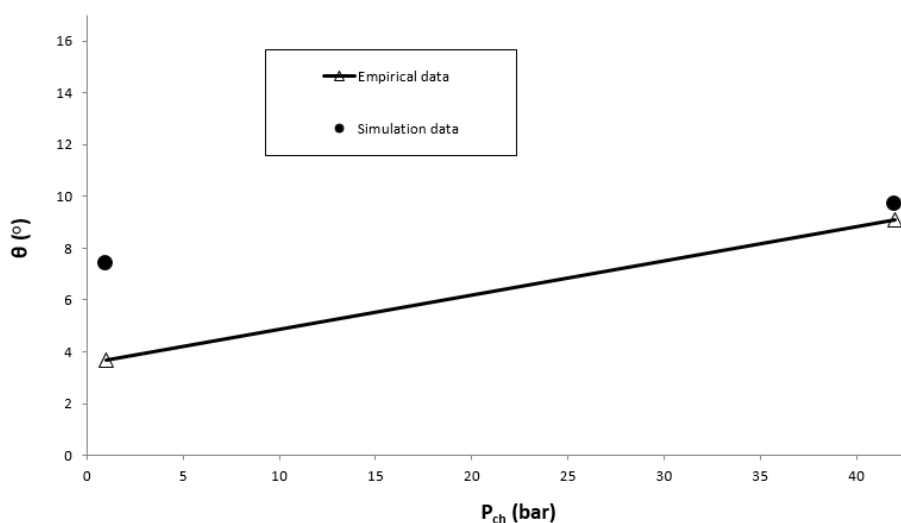


Figure 10. Comparison of the spray angle between simulation and empirical data at 0.25 ms ASOI for increasing chamber pressure at 700 K chamber temperature.

The comparison of spray angle for high chamber pressure conditions and 700 and 1000 K is illustrated in Figure 11. Figure 11 shows that the same trend of a slight decrease of the spray angle when the chamber temperature is increasing occurs both for the empirical data and the simulation. The agreement of spray jet angle from the simulations with the empirical data is very good, and the spray angle is slightly underestimated in the simulations. Again, the underestimation can be explained by the evaporation phenomenon which takes place and reduces the radial dispersion of the predicted spray jet from the simulation.

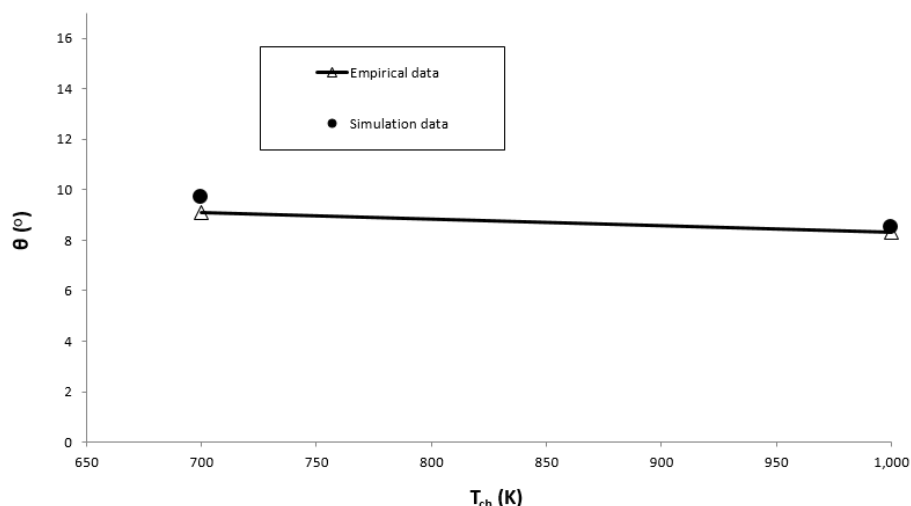


Figure 11. Comparison of the spray angle between simulation and empirical data at 0.25 ms ASOI for increasing chamber temperature at 42 bar chamber pressure.

For reaching definite conclusions and assess the validity of both the simulation and empirical data, detailed measurements of the liquid breakup length and the spray jet angle are required for the various chamber conditions examined in the present work. Furthermore, chamber conditions resembling diesel engine conditions, including high turbulence, exhaust gas residuals and exhaust gas recirculation are needed. Overall, the simulations performed in the present work captured the same trends with the empirical data and can provide meaningful results which can be used for diesel engine spray investigations and diesel engine combustion modelling setup, which should be complemented with the relevant combustion modelling methodologies including detailed and/or reduced chemical kinetics mechanisms configurations, for real fuels at high pressure and high temperature conditions.

Conclusions and recommendations

The effects of chamber pressure and chamber temperature on the initial diesel spray characteristics were examined by the use of two-phase flow simulations of a typical six-hole diesel injector injecting at very high pressure. The flow patterns within the nozzle and at the vicinity of the nozzle exit were simulated and compared for four test cases.

The main finding revealed that the effect of temperature on the spray jet is negligible, while the effect of chamber pressure on the liquid breakup length and spray jet angle is very strong. The comparisons with empirical data verified that the simulation captures the same trends for the liquid jet breakup length especially at the early stages of injection, as well as the spray jet angle values. The spray angle increases by around 50 % when the chamber pressures increases by 40 bar, and when the chamber temperature increases around 300 K the spray angle decreases around 10 %.

For future work, the methodologies of LES and DNS will be used in order to further examine the chamber conditions effect on the initial spray jet characteristics. However, it is further required to compare the simulations against detailed experimental data of sprays in both constant volume chambers with conditions resembling engine cylinder conditions with high levels of turbulence, as well as simulate the diesel spray injection in diesel engine cylinders, where the conditions of cylinder pressure and temperature are varying both during piston motion and from engine cycle-to-cycle.

Acknowledgements

The provision of computer facilities by Frederick University is acknowledged.

References

- [1] Andriotis, A, Gavaises, M. and Arcoumanis, C., 2008, *J. Fluid Mech.*, 60, pp. 195-215.
- [2] Arai, M., Sep. 2.-6. 2012, 12th Triennial International Conference on Liquid Atomization and Spray Systems.
- [3] Computational Dynamics adapco Ltd., 2015, STAR-CD Methodology, Version 4.22. London, England.
- [4] Dassault Systèmes SolidWorks Corporation, <http://www.solidworks.com>.
- [5] de Villiers, E., Gosman, A. D. and Weller, H. G., 2004, SAE Technical Paper Series 2004-01-0100.
- [6] Giannadakis, E., Gavaises, M. and Arcoumanis, C., 2008, *J. Fluid Mech.*, 616, pp. 153-193.
- [7] Heywood, J. B. 1987, "*Internal Combustion Engine Fundamentals*"

- [8] Jameel, A., Bowen, P., and Yokoi, K., 8.-10. Sep., 2014, 26th European Conference on Liquid Atomization and Spray Systems.
- [9] Margot, X., Hoyas, S., Fajardo, P. and Patouna, S., 2010, *Mathematical and Computer Modelling*, 52, pp. 1143-1150.
- [10] Oda, T., Ohnishi, K., Sumi, T. and Ohsawa, K., Sep. 2.-6. 2012, 12th Triennial International Conference on Liquid Atomization and Spray Systems.
- [11] Payri, F., Payri, R., Salvador, F. J. and Martinez-Lopez, J., 2012, *Computers & Fluids*, 58, pp.88-101.
- [12] Payri, F., Salvador, F. J., Marti-Aldaravi, M. and Martinez-Lopez, J., 2012, *Energy Conversion and Management*, 54, pp.90-99.
- [13] Salvador, F. J., Martinez-Lopez, J., Romero, J. V. and Rosello, M. D., 2013, *Mathematical and Computer Modelling*, 57, pp. 1656-1662.
- [14] Sou, A., Pratama, R. H., Tomisaka, T. and Kibayashi, Y., 2.-6. 2012, 12th Triennial International Conference on Liquid Atomization and Spray Systems.
- [15] Tamaki, N., Nishikawa, K. and Fukamichi, S., 1.-4. Sep.2013, 25th European Conference on Liquid Atomization and Spray Systems.
- [16] Varde, K. S., 1985, *The Canadian Journal of Chemical engineering* 63
- [17] Yakhot, V., and Orszag, S.A. 1986, *J. Scientific Computing*, 1, pp. 1–51.